Available online at www.sciencedirect.com

SciVerse ScienceDirect

Ceramics International 39 (2013) 5213–5218

CERAMICS INTERNATIONAL

www.elsevier.com/locate/ceramint

EDTA-assisted template-free synthesis and improved photocatalytic activity of homogeneous ZnSe hollow microspheres

Xiong Wang*, Li Li, Ying Lin, Juanjuan Zhu

School of Materials Science and Engineering, Nanjing University of Science and Technology, Nanjing 210094, China

Received 26 November 2012; received in revised form 6 December 2012; accepted 6 December 2012
Available online 14 December 2012

Abstract

Homogeneous ZnSe hollow microspheres were synthesized on a large scale through an EDTA-assisted mixed solvothermal strategy without any surfactants and templates. The as-synthesized ZnSe microspheres were characterized by X-ray diffraction (XRD), scanning electron microscopy (SEM), transmission electron microscopy (TEM), X-ray photoelectron spectroscopy (XPS), and UV–vis absorption spectroscopy. The results of photodegradation of methylene blue (MB) indicate that the hollow microspheres exhibit a visible-light-responsive photocatalytic behavior. As compared with the bulk ZnSe, the photocatalytic efficiency for the hollow microspheres was enhanced remarkably, which might be related with the hollow aggregates of ZnSe nanocrystallites.

Keywords: Hollow microspheres; Nanocrystallites; ZnSe; Photocatalytic

1. Introduction

Since Fujishima and Honda discovered the photocatalytic splitting of H_2O for TiO_2 in 1972 [1], heterogeneous photocatalysis of semiconductor materials has garnered an increasing amount of attention for its great potential applications in solar energy conversion and photodegradation of organic contaminants. Due to its good photostability and environmental benignity, TiO_2, as photocatalyst, has been intensively investigated over the past decade [2–4]. However, TiO_2 can only be irradiated under ultraviolet light resulting from its large band gap (3.2 eV, 388 nm). The poor solar energy utilization efficiency (less than 5%) impedes the practical application of TiO_2. Therefore, considerable efforts have been made to exploit novel visible-light-responsive photocatalysts, such as Bi-based ternary oxides [5–10], transition metal oxides [11–13], and semiconductor chalcogenide compounds [14,15]. Among them, ZnSe, as an important II–VI semiconductor with direct band gap of 2.70 eV (460 nm), has attracted extensive interest due to its wide applications in many fields like light-emitting diodes, biomedical sensors, and photocatalysts [16–19].

Due to the crystal structure, surface area and morphology of semiconductor materials greatly influence their electrical and optical properties, semiconductor nanomaterials exhibit improved photocatalytic performances. Nevertheless, it also brings about separation difficulty. Nanostructured photocatalyst assembled by nanoparticles can efficiently overcome these problems, simultaneously possessing enhanced photocatalytic activity and easy recovery. Herein, we report a facile EDTA-assisted synthetic strategy for fabrication of hollow ZnSe microspheres on a large scale. The microspheres were assembled by nanoparticles with average diameter of 80 nm. Hollow zinc selenide spheres were also prepared before by other research groups [20], using hydrazine hydrate as reductant and forming gas N_2 as template. In our template-free solvothermal synthesis, no strong reducing agents like $N_2H_4 \cdot H_2O$ were used, and hollow microspheres were formed by a symmetric Ostwald ripening. Under visible light irradiation, the enhanced photocatalytic behaviors of ZnSe hollow microspheres were evaluated by degradation of methylene blue (MB).

2. Experimental

All the chemicals were of analytical purity grade and were used as received without further purification. In a

*Corresponding author. Tel./fax: +86 25 8431 3349.
E-mail address: xiongwang@njust.edu.cn (X. Wang).

0272-8842/$ - see front matter © 2012 Elsevier Ltd and Techna Group S.r.l. All rights reserved.
http://dx.doi.org/10.1016/j.ceramint.2012.12.020

typical procedure, 4.0 g (0.1 mol) of NaOH and an appropriate amount of EDTA were firstly dissolved into 30 mL deionized water. Then, 0.549 g (2.5 mmol) of $Zn(CH_3COO)_2 \cdot 2H_2O$ and 0.433 g (2.5 mmol) of Na_2SeO_3 were added into the solution under magnetic stirring until a transparent solution was obtained. Finally, 90 mL of ethylene glycol (EG) was poured into the above solution. After stirring for 10 min, the transparent solution was transferred into a Teflon-lined stainless steel autoclave, sealed and maintained at 180 °C for 12 h. After the reaction, the autoclave was cooled down to room temperature naturally. The final product was collected by centrifugation, washed repeatedly with deionized water and absolute ethanol in an ultrasonic bath, vacuum-dried at 80 °C, and kept for further characterizations.

The crystalline phase was identified by X-ray diffraction (XRD) using a Philips X'Pert Pro Super diffractometer with Cu K_α radiation ($\lambda = 1.541784$ Å). The morphology of the sample was examined by scanning electron microscope (SEM, Hitachi, X-650) and transmission electron microscope (TEM, JEOL, JEM-2010). For the TEM observation, the products were dispersed by sonication in absolute ethanol, and the obtained colloid suspension was dripped on the TEM copper mesh. X-ray photoelectron spectrum (XPS) was collected on an ESCALab MKII X-ray photoelectron spectrometer, using nonmonochromatized Mg K_α X-ray as the excitation source and C 1 *s* (284.6 eV) as the reference line. UV–vis absorption spectrum of the sample was obtained on a Shimadzu UV2450 UV–vis spectrophotometer equipped with an integrating sphere.

The photocatalytic activity of the samples was evaluated by photodegradation of methylene blue at room temperature. The light source was a 500 W Xe lamp positioned in a quartz cold trap which was in the middle of multiposition cylindrical reaction vessel. Appropriate cutoff filters were placed around the cold trap to ensure complete removal of radiation below 400 nm and to ensure that the catalysis process occurred only under visible light. The system was cooled by wind and water and was maintained at the room temperature. 10 mg of ZnSe microspheres as photocatalyst was added to 10 mL methylene blue solution (10^{-5} mol L^{-1}) in the vessel. Before irradiation, the suspensions were stirred in the dark for 1 h to ensure the establishment of an adsorption–desorption equilibrium between the photocatalyst and methylene blue. Then the solution was exposed to visible light irradiation under stirring. At given time intervals, 3 mL suspensions were sampled and centrifuged to remove the photocatalyst particles. Then, the UV–vis absorption spectrum of the centrifugated solution was recorded by the UV2450 UV–vis spectrophotometer.

3. Results and discussion

3.1. XRD analysis

The phase structure of the products was examined by powder X-ray diffraction. Fig. 1 shows the XRD patterns of the powders prepared hydrothermally at different ratios of EDTA to Zn. All diffraction peaks of the samples can be indexed to face-centered cubic blende structure of ZnSe with a lattice constant of $a = 5.628$ Å, matching well with the standard powder diffraction data (JCPDS card no. 80-0021). Peaks arising from impurities are not observed, indicating the high purity of the final product. With increasing the EDTA/Zn ratio from 0 to 2, all the XRD patterns are similar. The diffraction intensity varies almost imperceptibly as well as the peak width (Fig. 1a–d). The average grain size is estimated by Scherrer's formula after making correction for the instrumental broadening which is equal to 65 nm.

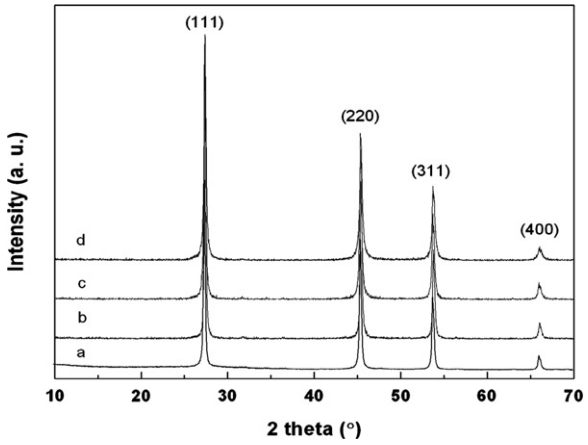

Fig. 1. XRD patterns of ZnSe microspheres prepared hydrothermally at 180 °C for 12 h at different EDTA/Zn ratios: (a) 0, (b) 1, (c) 1.5 and (d) 2.

3.2. Morphological analysis

The morphology of the obtained ZnSe powders were characterized by scanning electron microscopy (SEM) and transmission electron microscope (TEM). The roughness of the particle surfaces, which can be observed from the SEM images (Fig. 2), suggests that the particles are not single crystalline. Without adding EDTA, the morphologies of the powders are diverse (Fig. 2a), including microspheres and irregular particles. With the increment of EDTA, the spherical particles are gradually predominant, and ultimately other shapes disappear. On further observation of the sample shown in Fig. 2(d), the hollow spherical feature could be obviously noticed from these broken microspheres.

To further confirm the hollow sphere character of the particles, the as-prepared microspheres at EDTA/Zn ratios equal to 2 were re-dispersed in absolute alcohol, sonicated for half an hour and sampled. Fig. 3 exhibits the morphology of the sample, depicting the homogeneous spherical morphology with an average diameter of 1.2 μm and a fairly narrow size-distribution. A TEM image of the typical microsphere after sonication is presented in Fig. 3(c). The intense contrast between the black margins and the bright centers of the particles confirms the

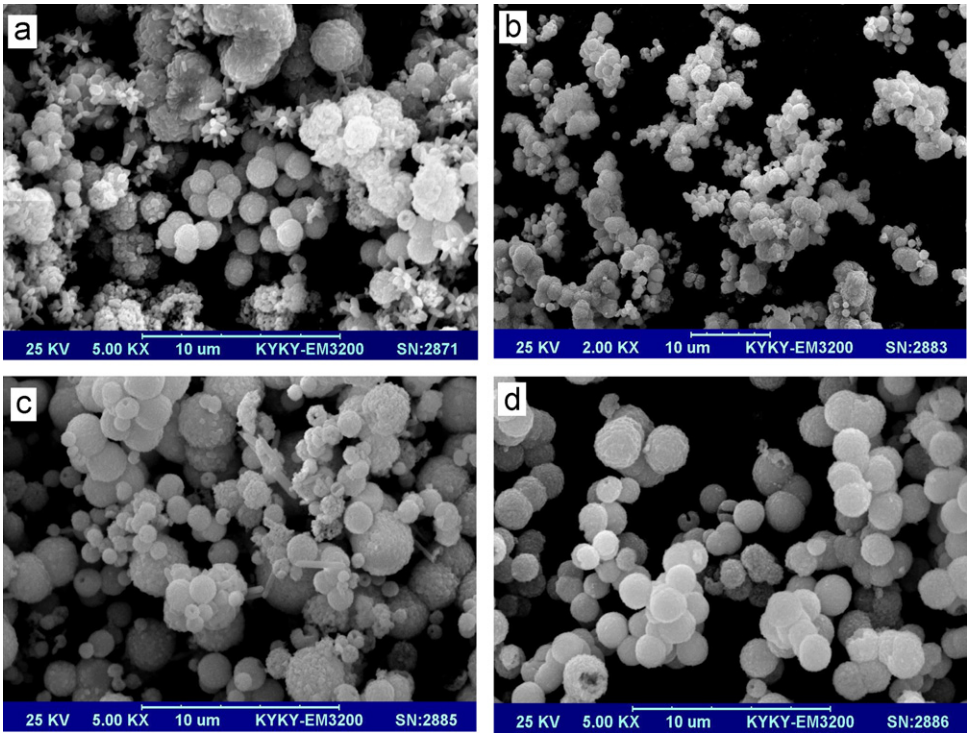

Fig. 2. SEM images of the as-obtained microspheres at EDTA/Zn ratios of (a) 0, (b) 1, (c) 1.5 and (d) 2, respectively.

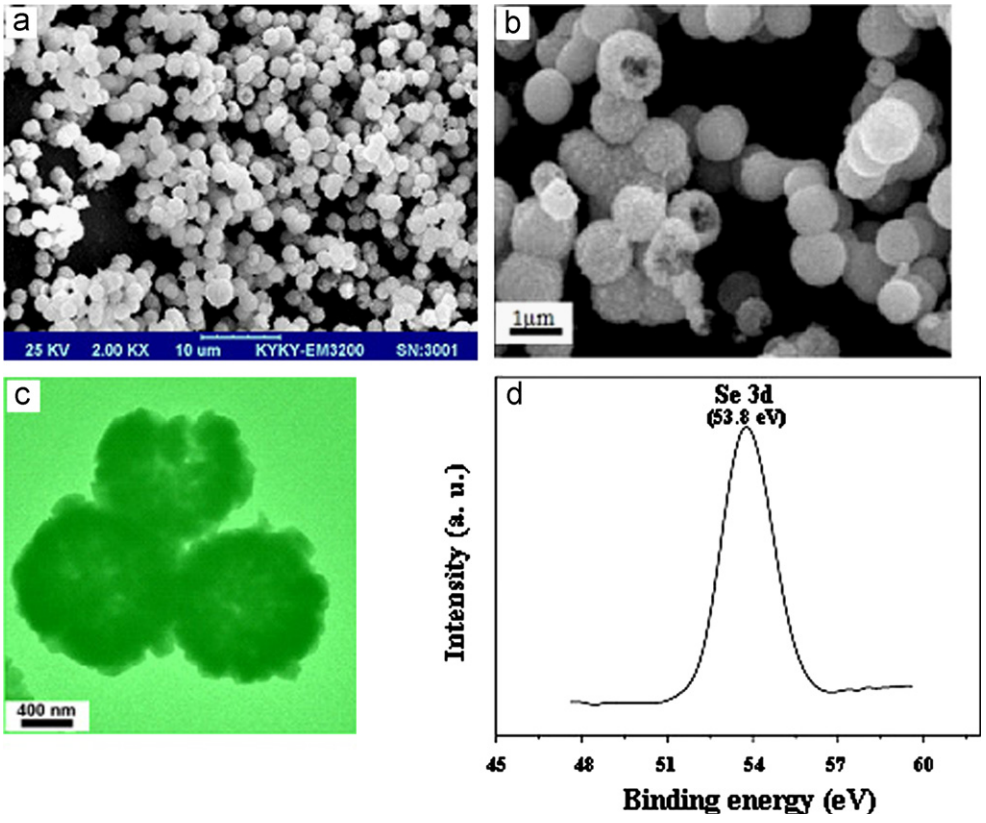

Fig. 3. (a) SEM image showing the overall product morphology, (b) Magnified SEM, (c) TEM images of the resulting products, clearly exhibiting the uniform hollow spherical morphology and (d) XPS core spectrum of Se 3d for the powders.

existence of hollow features in the resulting microspheres, which is consistent with the SEM observation. The shells of the hollow spheres are composed of numerous nanocrystals with an average size of 80 nm, and shell thickness of about 200 nm. The symmetrical Se 3d XPS core spectrum (Fig. 3d) of the sample reveals the binding energy as 53.8 eV, further identifying the hollow microspheres as pure ZnSe instead of elementary substance Se.

3.3. Formation mechanism

Because the properties of nanosized materials are strongly influenced by their shape, it is very important to explore the growth mechanism. In principle, the process involves reacting zinc salt solutions with selenite, which is reduced in glycol environment and releases Se^{2-} ions. The sequence of chemical processes involved in the formation of ZnSe particles is presented below:

$$HOCH_2CH_2OH = CH_3CHO + H_2O \quad (1)$$

$$2CH_3CHO + SeO_3^{2-} = 2CH_3COO^- + Se + H_2O \quad (2)$$

$$3Se + 6OH^- = 2Se^{2-} + SeO_3^{2-} + 3H_2O \quad (3)$$

$$Zn^{II}(EDTA) + Se^{2-} \rightarrow ZnSe \quad (4)$$

It is worthwhile to note that the quantity of EDTA has strong effects on the formation of uniform well-defined hollow spherical morphology. With increasing the EDTA/Zn ratio, the dominant product remains regular microspheres. When the ratio is up to 2, the hollow microspheres are the only morphology. The formation mechanism of ZnSe hollow microspheres is believed to be Ostwald ripening process involving "the growth of larger crystals from those of smaller size which have a higher solubility than the larger ones" [21]. The process is illustrated in Scheme 1. After the initial nucleation, the poorly crystallized ZnSe primary particles aggregate together to form solid microspheres driven by the minimization of the total energy in the system. Under the present condition, there is a crystallite-size distribution or particle density gradient across the solid [22]. The smaller interior crystallites with a higher solubility will dissolve and a core hollowing process starts. With the increase of reaction time, the inner core is completely consumed and the crystallinity of the products increases gradually.

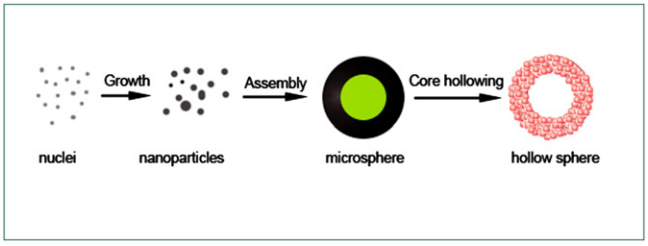

Scheme 1. Sketch of the proposed growth mechanism of the ZnSe hollow microspheres.

3.4. Optical properties

Fig. 4 shows the UV–vis absorption spectrum of the ZnSe hollow microspheres. A steep absorption edge at about 400 nm was observed, which was attributed to the interband transition or exciton absorption of the nanoparticles. For the direct band gap semiconductor ZnSe, the absorption band gap E_g can be determined by the equation $(\alpha h\nu)^2 = B(h\nu - E_g)$, where α, h, ν, E_g and B is absorption coefficient, Planck constant, light frequency, band gap, and a constant, respectively. The band gap is estimated about 2.9 eV (427.5 nm) by the linear extrapolation (as shown in Fig. 4b), a small hypsochromic shift observed as compared to bulk ZnSe (2.6–2.8 eV) [18,23]. Hence, the resulting ZnSe hollow microspheres might have a potential application as photocatalyst in the expanded visible-light region.

Within the ecosystem, this colored wastewater is a dramatic source of pollution, eutrophication, and perturbations in aquatic life. To evaluate the photocatalytic activity of the hollow microspheres, methylene blue was chosen as the model pollutant to determine the photocatalytic efficiency, and the photodegradation of methylene

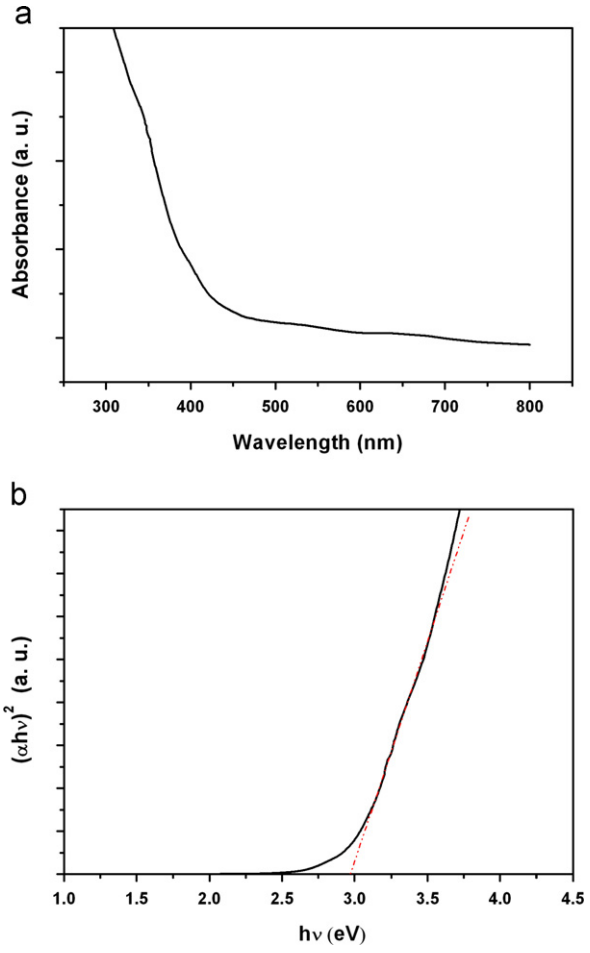

Fig. 4. UV–vis absorption spectrum (a) and the corresponding $(\alpha h\nu)^2$–$h\nu$ plot (b) of the ZnSe hollow microspheres.

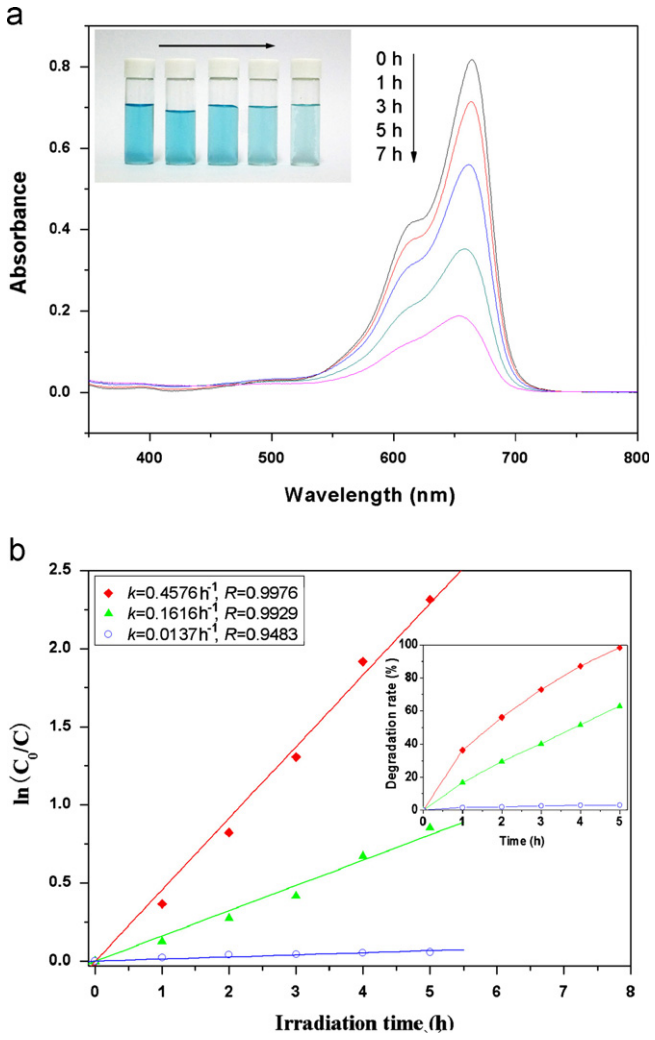

Fig. 5. (a) Absorption changes of methylene blue solution irradiated under visible light in the presence of ZnSe hollow microspheres. (b) The degradation kinetics of MB in the presence of the bulk ZnSe (circle), the solid (filled triangle) and the hollow ZnSe microspheres (filled square), respectively. The inset shows the corresponding photodegradation rate.

blue solution was conducted under visible light irradiation ($\lambda > 400$ nm). Fig. 5(a) exhibits the temporal evolution of the absorption spectrum with the hollow microspheres as photocatalyst. During the photodegradation, the characteristic absorption of MB at 664 nm decreased remarkably with the irradiation time. The color-change sequence is shown in the inset of Fig. 5(a). It is clear that the intense color of the starting solution gradually decreases with increasing the exposure time.

Fig. 5(b) displays time profiles of lnC_0/C under visible light irradiation, where C was the concentration of MB at the irradiation time t and C_0 was the concentration after the adsorption equilibrium on ZnSe at $t=0$. As observed from the figure, the lnC_0/C linearly increased with the irradiation time, indicating that the photodegradation of MB over ZnSe could be described as first-order reaction. Therefore, the photocatalytic activities can be evaluated by the apparent first-order rate constant k. From the kinetic plots and the degradation rate curves, the bulk ZnSe hardly exhibits photocatalytic activity under visible light irradiation. As compared with that of the bulk ZnSe ($k=0.0137\ h^{-1}$), the photocatalytic activity of the solid ZnSe microspheres obtained at the EDTA/Zn ratio of 1 was improved by about 11.8 times ($k=0.1616\ h^{-1}$), the hollow microspheres by about 33.4 times ($k=0.4576\ h^{-1}$). The improvement of the photocatalytic efficiency might be attributed to the hollow aggregates of ZnSe nanocrystallites, which results in an increase of catalytic/reactive sites related with specific surface area and an enhancement of the redox potential of the photoinduced electron–hole pairs.

4. Conclusions

Homogeneous ZnSe hollow microspheres were successfully synthesized through an EDTA-assisted mixed solvothermal strategy on a large scale. The ZnSe nanoparticles aggregate to form the hollow structure by Ostwald ripening process, in which EDTA plays a vitally important role. Taking the process one step further, we can make extensive use of this method to synthesize a wide variety of semiconductive materials. The results of photocatalysis indicate that the hollow microspheres possess the visible-light-responsive photocatalytic activity. As compared with the bulk ZnSe, the photocatalytic efficiency for the hollow microspheres was enhanced remarkably, which might be related with the hollow aggregates of ZnSe nanocrystallites.

Acknowledgments

We gratefully acknowledge the financial supports from the National Natural Science Foundation of China (21001064), the Natural Science Foundation of Jiangsu Province (BK2010487), the Specialized Research Fund for the Doctoral Program of Higher Education of China (20103219120045), and the NUST Research Funding (2011ZDJH27).

References

[1] A. Fujishima, K. Honda, Electrochemical photolysis of water at a semiconductor electrode, Nature 238 (1972) 37–38.
[2] T. Kawahara, Y. Konishi, H. Tada, N. Tohge, J. Nishii, S. Ito, A patterned TiO_2(anatase)/TiO_2(rutile) bilayer-type photocatalyst: effect of the anatase/rutile junction on the photocatalytic activity, Angewandte Chemie International Edition 41 (2002) 2811–2813.
[3] W.J. Stark, K. Wegner, S.E. Pratsinis, A. Baiker, Flame aerosol synthesis of vanadia–titania nanoparticles: structural and catalytic properties in the selective catalytic reduction of NO by NH_3, Journal of Catalysis 197 (2001) 182–191.
[4] G. Miao, L. Chen, Z.W. Qi, Facile synthesis and active photocatalysis of mesoporous and microporous TiO_2 nanoparticles, European Journal of Inorganic Chemistry (2012) http://dx.doi.org/10.1002/ejic.201200833.
[5] M. Shang, W.Z. Wang, H.L. Xu, New Bi_2WO_6 nanocages with high visible-light-driven photocatalytic activities prepared in refluxing EG, Crystal Growth and Design 9 (2009) 991–996.

[6] X. Wang, Y. Lin, X.F. Ding, J.G. Jiang, Enhanced visible-light-response photocatalytic activity of bismuth ferrite, Journal of Alloys and Compounds 509 (2011) 6585–6588.
[7] J.W. Tang, Z.G. Zou, J.H. Ye, Photocatalytic decomposition of organic contaminants by Bi_2WO_6 under visible light irradiation, Catalysis Letters 92 (2004) 53–56.
[8] A. Feteira, D.C. Sinclair, Microwave dielectric properties of low firing temperature $Bi_2W_2O_9$ ceramics, Journal of the American Ceramic Society 91 (2008) 1338–1341.
[9] X. Wang, Y. Zhang, Z.B. Wu, Magnetic and optical properties of multiferroic bismuth ferrite nanoparticles by tartaric acid-assisted sol–gel strategy, Materials Letters 3 (2010) 486–488.
[10] X. Chen, C. Ma, X. Li, P. Chen, J. Fang, Hierarchical Bi_2CuO_4 microspheres: hydrothermal synthesis and catalytic performance in wet oxidation of methylene blue, Catalysis Communications 10 (2009) 1020–1024.
[11] Z. Yang, D. Han, D. Ma, H.L. Liu, Y.Z. Yang, Fabrication of monodisperse CeO_2 hollow spheres assembled by nano-octahedra, Crystal Growth and Design 10 (2010) 291–295.
[12] G. Xi, Y. Yan, Q. Ma, J. Li, H. Yang, X. Lu, C. Wang, Synthesis of multiple-shell WO_3 hollow spheres by a binary carbonaceous template route and their applications in visible-light photocatalysis, Chemistry—A European Journal 18 (2012) 13949–13953.
[13] D.L. Chen, L. Gao, A. Yasumori, K. Kuroda, Y. Sugahara, Size- and shape-controlled conversion of tungstate-based inorganic–organic hybrid belts to WO_3 nanoplates with high specific surface areas, Small 4 (2008) 1813–1822.
[14] J. Jiang, H. Li, L.Z. Zhang, New insight into daylight photocatalysis of AgBr@Ag: synergistic effect between semiconductor photocatalysis and plasmonic photocatalysis, Chemistry—A European Journal 18 (2012) 6360–6369.
[15] X.H. Yang, X. Wang, Z.D. Zhang, Facile solvothermal synthesis of single-crystalline Bi_2S_3 nanorods on a large scale, Materials Chemistry and Physics 1 (2006) 154–157.
[16] S.L. Xiong, J.M. Shen, Q. Xie, Y.Q. Gao, Q. Tang, Y.T. Qian, A precursor-based route to ZnSe nanowire bundles, Advanced Functional Materials 15 (2005) 1787–1792.
[17] X. Wang, J. Zhu, Y. Zhang, J. Jiang, S. Wei, One-pot synthesis and optical properties of monodisperse ZnSe colloidal microspheres, Applied Physics A 99 (2010) 651–656.
[18] B. Xiang, H.Z. Hang, G.H. Li, F.H. Yang, F.H. Su, R.M. Wang, J. Xu, G.W. Lu, X. Xun, Q. Zhao, D.P. Yu, Green light emitting ZnSe nanowires fabricated via vapor phase growth, Applied Physics Letters 82 (2003) 3330–3332.
[19] H. Gong, H. Huang, M. Wang, K. Liu, Characterization and growth mechanism of ZnSe microspheres prepared by hydrothermal synthesis, Ceramics International 33 (2007) 1381–1384.
[20] Q. Peng, Y.J. Dong, Y.D. Li, ZnSe semiconductor hollow microspheres, Angewandte Chemie International Edition 42 (2003) 3027–3030.
[21] W. Ostwald, Uber die vermeintliche Isomeric des roten und gelben Quecksilberoxyds und die Oberflachenspannung gester Korper, Zeitschrift für Physikalische Chemie 34 (1900) 495–503.
[22] B. Liu, H.C. Zeng, Symmetric and asymmetric Ostwald ripening in the fabrication of homogeneous core–shell semiconductors, Small 5 (2005) 566–571.
[23] S.K. Hong, E. Kurts, J.H. Chang, T. Hanada, M. Oku, T. Yao, Low stacking-fault density in ZnSe epilayers directly grown on epi-ready GaAs substrates without GaAs buffer layers, Applied Physics Letters 78 (2001) 165–167.